HUNTINGTON MEDICAL RESEARCH INSTITUTES
NEUROLOGICAL RESEARCH LABORATORY
734 Fairmount Avenue
Pasadena, California 91105

5-2333

Contract No. NO1-NS-2333

QUARTERLY PROGRESS REPORT

Jan 1 - March 31, 1998

Report No. 10

"Microstimulation of the Lumbosacral Spinal Cord"

William F. Agnew, Ph.D.
Douglas B. McCreery, Ph.D.
Albert Lossinsky. Ph.D
Leo Bullara. B.A.

THIS QPR IS BEING SENT TO YOU BEFORE IT HAS BEEN REVIEWED BY THE STAFF OF THE NEURAL PROSTHESIS PROGRAM.

INTRODUCTION

At Huntington Medical Research Institutes, we have been developing electrodes and protocols for safe, prolonged microstimulating in the mammalian central nervous system, using arrays of chronically-implanted microelectrodes. We have developed these methodologies to the point where microelectrodes can be implanted chronically into the feline cerebral cortex and into the cochlear nucleus of experimental animals with a minimum of tissue injury, and we have made considerable progress in the development of protocols for prolonged stimulation with arrays of closely-spaced microelectrodes. In the spinal cord, we have encountered some problems of electrode instability and tissue injury that appear to be related to the special environment of this site, and we have undertaken a series of studies to identify and remedy these problems.

One source of difficulty appears to be related to the rostral-caudal movement of the cord relative to the dura as the animal extends its hindlimbs or arches its back, and this may be linked to the manner in which the electrode cables are secured. The deformation of the tissue around the rigid microelectrode shafts during closure of the dura after electrode implantation may also contribute to the tissue injury. We have observed that the evoked responses recorded from the ventral roots and the elevations in bladder pressure induced by intraspinal microstimulation often change markedly after the dura is sutured over newly-implanted individual microelectrodes. This implies that the manipulation of the array during suturing of the dura may contribute to the displacement of the electrodes and hence to the tissue injury. However, the dura must be closed in some fashion to prevent leakage of CSF, and to keep the array from drifting up out of the cord. Also, the method of closure must not encourage the spinal roots or the subdural segment of the cable to become entrapped within connective tissue. Our new 3-electrode arrays may be more stable during the suturing process than are the single microelectrodes that we have used previously, and we are investigating the merits of closing the dura with sutures after implantation of the electrode array and, alternatively, of patching the opening with a sheet of fascia.

METHODS

Four adult male cats (sp89, sp90, sp91, and sp92) were anesthetized with a mixture of 50% nitrous oxide and 1.5-2.0% Halothane. The spinal cord was exposed from the L_6 to S_3 root level with a standard dorsal laminectomy. The S_2 level of the spinal cord is located by stimulating electrically the dermatome innervated by the S_2 root (the perigenital region) as a recording electrode is passed over the dorsal surface of the cord. The cord level at which the maximum evoked response is recorded indicates the middle of the S_2 segment of the cord. A longitudinal incision was made through the dura at this level. The arachnoid was then dissected from the dorsal roots. The dorsal spinal process anterior to the laminectomy was secured with a vertebral clamp.

The electrode arrays contained 3 activated iridium microelectrodes, the lengths of which were either 1.1, 1.2 and 1.3 mm, (sp89, sp90), or 1.2, 1.3 and 1.4 mm (sp91). The microelectrodes themselves were 35 μm in diameter and were insulated with Epoxylite electrode varnish. The microelectrodes are 500 μm apart, and extend from an epoxy matrix 2 mm in length and approximated 0.75 mm in width. The tips were quite blunt (radius of curvature of 5 to 6 μm) in order to minimize injury to the microvasculature of the spinal cord. These arrays did not have cables, since it is part of our strategy to examine the role of the cables in the displacement of the arrays. In later animals, the arrays will have cable, and we will examine two different means of stabilizing them, so that they do not dislodge the electrodes.

Two arrays of three iridium microelectrodes were implanted into each cat, using an axial introducer. During insertion, a vacuum holds the top of the array against the orifice of the introducer. The arrays were inserted into the dorsal columns at an angle of 26° from the vertical. The target was the lateral cell column of the preganglionic parasympathetic nucleus, which innervates the bladder detrusor muscle. The system is designed so that the electrodes can be inserted into the cord precisely on axis and thus minimize the chance of slashing the tissue.

In cats sp89 and sp90, the spinal dura was not sutured closed after insertion of the arrays, but a patch of fascia was placed over the cord prior to closing the

musculature over the laminectomy. In cat sp91, and sp92, the dura was closed loosely with three 7-0 sutures, and a fascia patch was placed over the loose dural closure.

Thirty days after implantation of the arrays, the cats were sacrificed for histologic evaluation of the electrode sites. The animals were deeply anesthetized, then perfused through the aorta with saline followed by 1.5 liters of ½ strength Karnovsky's fixative. The sacral cord and spinal roots were dissected out, the connective tissue overlying the array matrices was shaved away, and the microelectrodes were removed from the cord. The tissue was embedded in paraffin. Sections were stained with H&E and Nissl. The primary goal of these studies is to assess the electrode's positional stability and the related tissue injury, and the thick (8-10 μm) paraffin sections are more than adequate for this purpose. The use of paraffin embedding and the thicker sections considerably shorten the time required for histologic processing.

RESULTS

We describe the findings from cats sp89, sp90 and sp91. Cat sp92 is yet to be sacrificed, and the findings will be presented in the next report.

Gross Observations: There was considerably less connective tissue on the dorsal surface of the spinal cord in the two animals in which the dura was not sutured over the the spinal cord (sp89, sp90 - Fig. 1). In sp91, we found a thickened connective tissue layer covering the dura. The thickened layer made dissecting more laborious compared to the animals in which the cord was covered with fascia. There was no evidence of hemorrhage in any of the three animals.

Histological Observations: In some of the animals, there was compression of the dorsal surface of the cord, produced by the matrices of the electrode arrays (Fig. 2). The lengths and diameters of the electrodes essentially delimited the depth and extent of the injury near their tracks. For example, the shorter electrodes (sp89) induced injury limited primarily to the dorsal white matter. White matter changes in this animal included edematous and/or myelin degeneration with occasional lipid-laden machrophages. The myelin changes occasionally extended into the tissue surrounding

the electrode sheath (Fig. 3). In animals in which the gray matter of the right or left gray dorsal horns was penetrated, we observed spongiform changes, and vascular hyperplasia, astrogliosis, and glial sheaths of variable thickness surrounding the electrodes (Figs. 4, 5). Associated with one electrode in sp91, we observed a large and widespread area of hemosiderin pigments in the dorsal portion of the cord, but some distance from the electrode tip. The hemosiderin was observed within macrophages and within the extracellular space (Figs. 6, 7). We did not observe microcavitations of the gray matter associated with the hemosiderin deposits. Some capillaries in this area demonstrated vasculitis, while other vessels presented a mild perivascular infiltrate consisting of small lymphocyte and mononuclear cells (Fig. 8). Neutrophils were occasionally observed within the neuropil. The electrode sheaths were composed of layers of collagen bundles of varying thickness intermixed with fibroblasts, mononuclear cells and few lymphocytes. Along some regions of the electrode sheaths, there were clumps of what appeared to be multinucleated giant cells, some of which appeared as large, complex formations (Figs. 9, 10).

In all three animals, neuronal injury was, by and large, unremarkable (Fig. 11). Nissl stain showed minimal dispersion or clumping of endoplasmic reticulum within the neurons immediately adjacent to the electrode tips (Figs. 12-14). H&E stain also indicated a few slightly darkened neurons adjacent to the electrode sheaths and/or electrode tips (Fig. 8). Dark, shrunken neurons were not observed. In all animals, reactive astrocytes were prominent surrounding the electrode sheaths and adjacent to the tips (Figs. 4, 5, 8, 10). There was little evidence of leukocytic infiltration associated with any of the electrode tips. One of the electrode sheaths, however, demonstrated a leukocytic infiltrate. This sheath was observed to include an extension of the pial membrane which appeared to have been dragged down into the cord during electrode insertion (Figs. 15-18). This electrode sheath contained neutrophils intermixed with fibrocytes and larger mononuclear cells.

DISCUSSION AND FUTURE PERSPECTIVES

Our results showed that arrays of 3 blunt-tipped iridium microelectrodes, with tip

diameters of approximately 10 to 12 μm, can be inserted into the sacral spinal cord without inducing interstitial microhematomas. The neurons near the tips appeared to be essentially normal, with minimal changes in the neuropil and neurons surrounding the tips. This is a considerable improvement over our previous results, in which there was often extensive tissue injury and glial scarring around the microelectrode tips. However, these blunt microelectrodes induced marked displacement and rotation of the cord as they were being inserted. There was little evidence that the microelectrodes had migrated through the tissue during the 30 days *in vivo*. However, the marked displacement and rotation of the cord during array insertion caused the electrode's trajectory to be considerably different from that intended and may have been responsible for some injury to the microvascualture. The arrays were inserted at a angle of 26° from the vertical so as to enter the lateral cell column of the preganglionic parasympathetic nucleus. However, due to the rotation of the cord during insertion, their actual trajectory was nearly vertical anatomically. There also were old glial scars and the isolated presence of hemosiderin adjacent to and distant from one of the microelectrode shafts. This observation suggests that there was some slashing of the tissue during insertion of the electrodes, as would occur if the pia were to be stretched and dragged down into the cord during the insertion process. Hemosiderin presence at some distance from the electrode tip also suggests that it may have been caused by the cord having been stretched during electrode insertion. Stretching, therefore, could likely have ruptured small blood vessels.

In the next series, we will implant arrays of microelectrodes with tips that are somewhat sharper, with radii of curvature of 1.5 to 2 μm, and these will more easily penetrate the pia and thus will produce less dimpling and rotation of the cord. It is our experience that sharper microelectrodes with piercing tips tend to induce interstitial microhematomas in the cerebral cortex and in the cochlear nucleus, but we have not examined this issue systematically in the spinal cord. We will determine if sharper microelectrodes induce microhematomas in the spinal cord, and if they do, we will have to determine a means of inserting the blunt-tipped electrodes through the pia without causing excessive dimpling and cord rotation. It may be possible to excise the pia prior

to inserting the microelectrodes. Another approach would be to increase the lubricity of the exterior surface of the electrodes by coating them with lipophilic substances. In this way, it would be theoretically possible to reduce drag as they are inserted through the white matter.

In this series, with the exception of increased fibrosis, there did not appear to be any adverse effect of suturing the dura over the microelectrode array. However, there is certain to be less manipulation of the inserted array, and less chance of tissue injury if the dura is not sutured. Since our procedure of patching the un-sutured dura with fascia appears to have worked well, we will continue to use this approach in the future series.

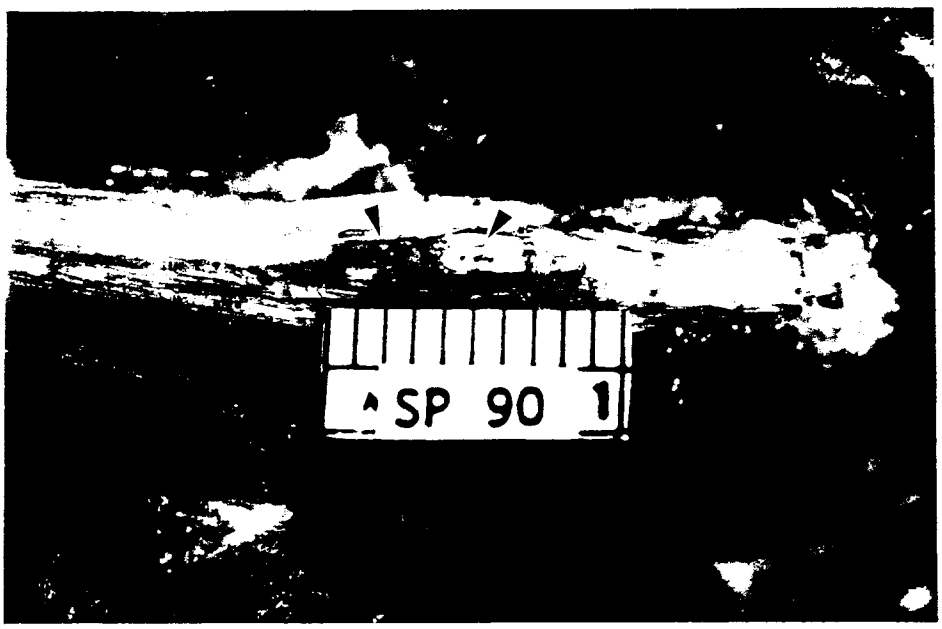

Fig. 1. Sp90. The surfaces of two matrices consisting of three electrode arrays are shown on the dorsal surface of the spinal cord (arrowheads).

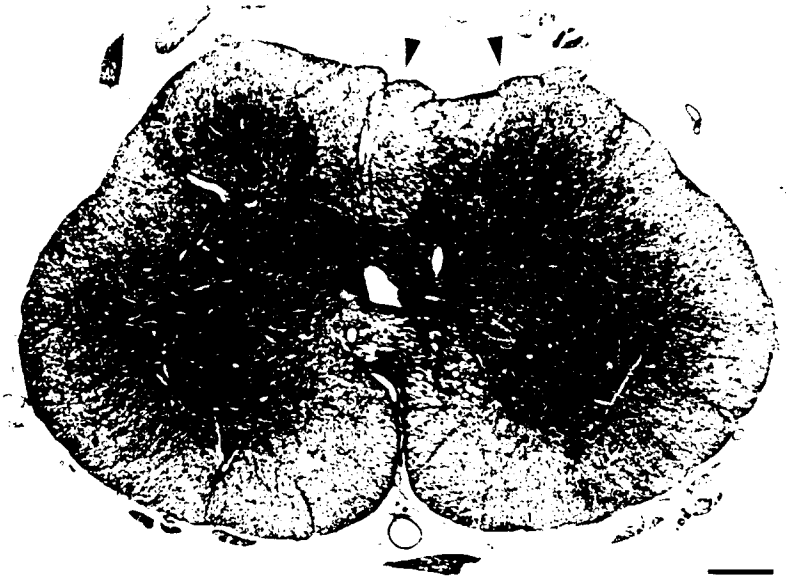

Fig. 2. Panoramic view of a section of the sacral spinal cord in sp91. Note the dorsal compression produced by the matrix of a three electrode array (arrowheads). Bar = 500 µm.

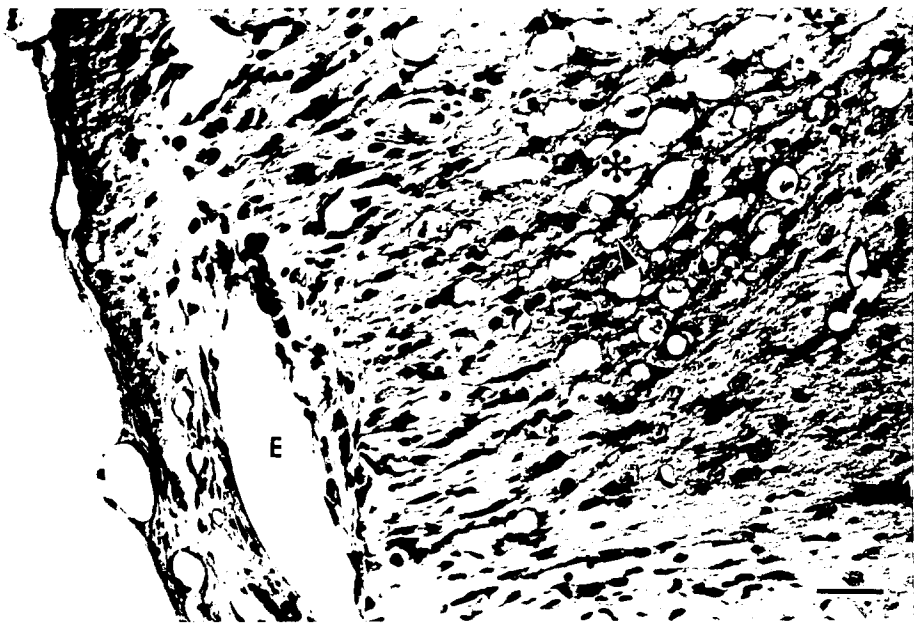

Fig. 3. Sp90. Moderate spongiosus (*) of the myelinated axons surrounding the electrode track (E) is shown. Scattered lipid-laden macrophages are shown nearby (arrowhead). Bar = 50 µm.

Fig. 4. Sp 89. The electrodes (E) produce several changes in the neuropil shown here including reactive astrocytes (arrowheads), vascular hyperplasia (v) and moderate spongiosus (*) Bar = 50 µm.

Fig. 5. Sp89. The sheaths surrounding other electrodes present a thin glial capsule (*) surrounded by numerous reactive astrocytes (arrowheads) and minimal spongiosus and lipid-laden machrophages (arrow). Bar = 25 µm.

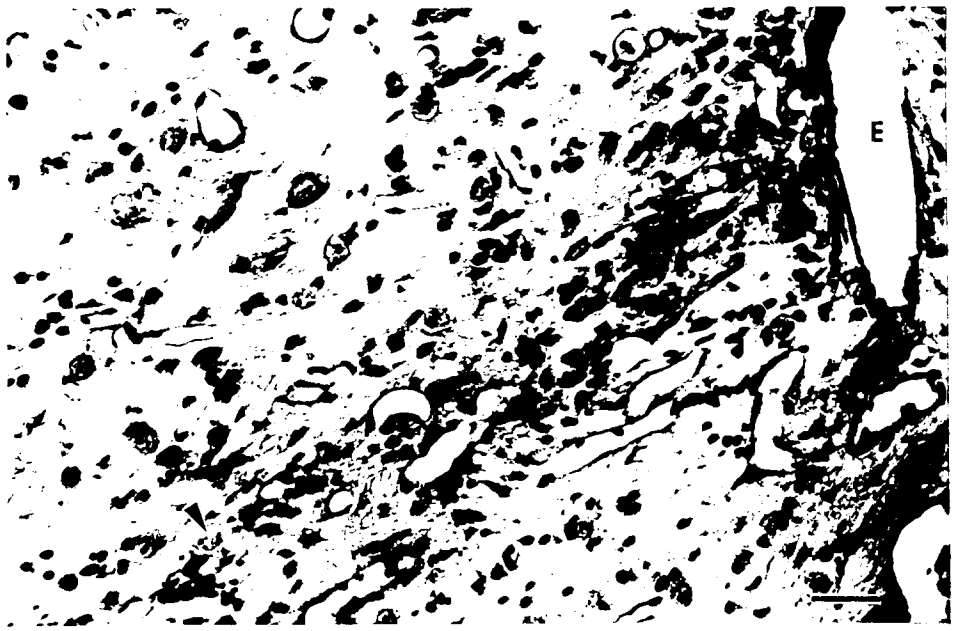

Fig. 6. Sp91. Hemosiderin pigments (arrowhead) are the remnants of an earlier hemorrhage. However, there is no evidence of gross microhematomas or microcavitations. The electrode track (E) is also shown. Bar = 50 μm.

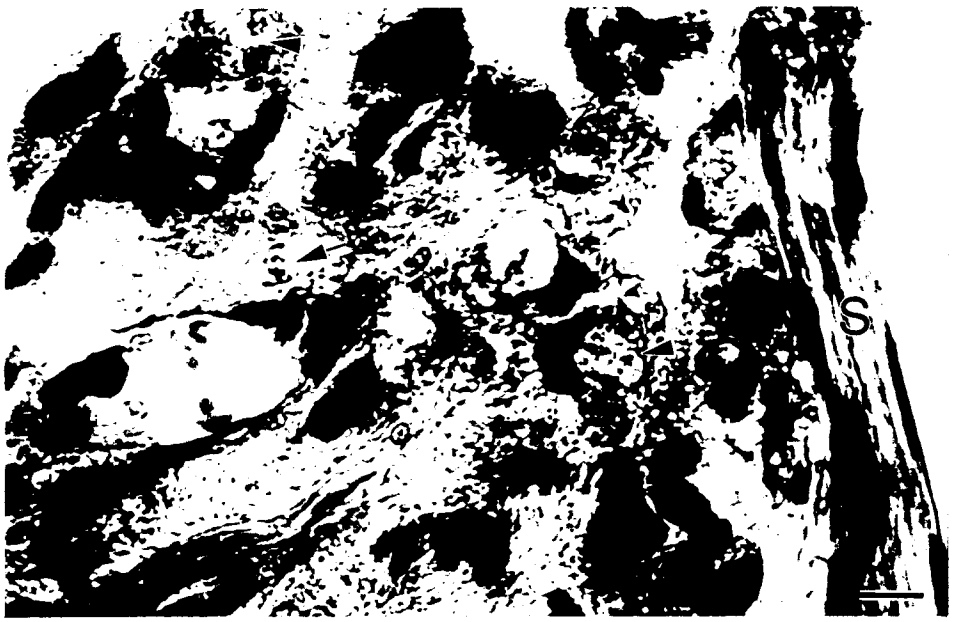

Fig. 7. Sp91. Higher magnification shows the hemosiderin deposits within large macrophages (arrowheads) and within the extracellular space (arrow) adjacent to the electrode sheath (S). Bar = 10 μm.

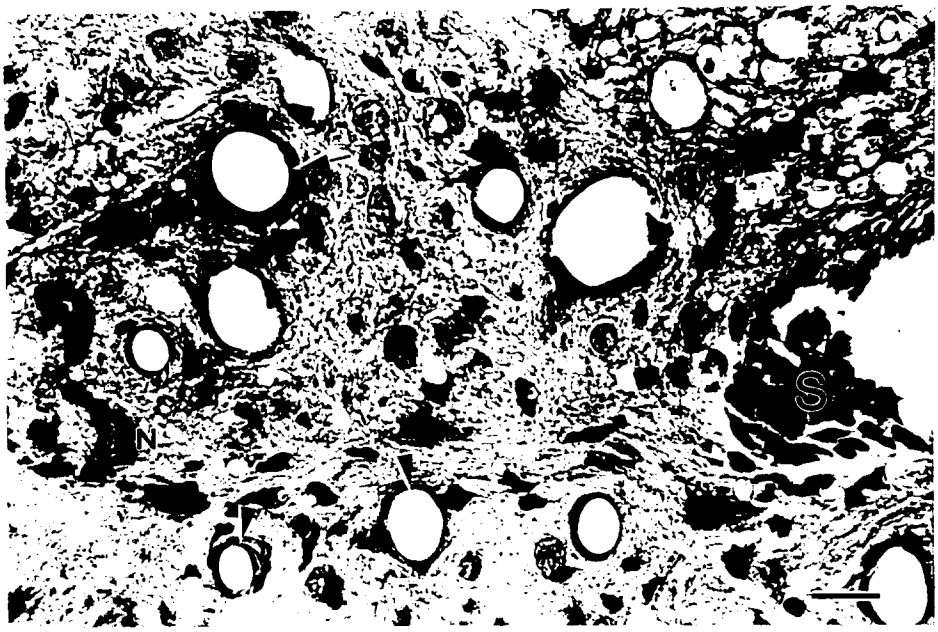

Fig. 8. Sp90. The region bordering the white and gray matter is shown adjacent to the edge of the electrode sheath (S). Note the clump of reactive astrocytes and mononuclear cells within the sheath. Two small blood vessels demonstrate slight thickening of their walls (arrowheads), while another vessel shows a vasculitis with a weak perivascular cuff (arrow) composed of a few small lymphocytes. Note also the slightly darkened neuron (N). Bar = 25 μm.

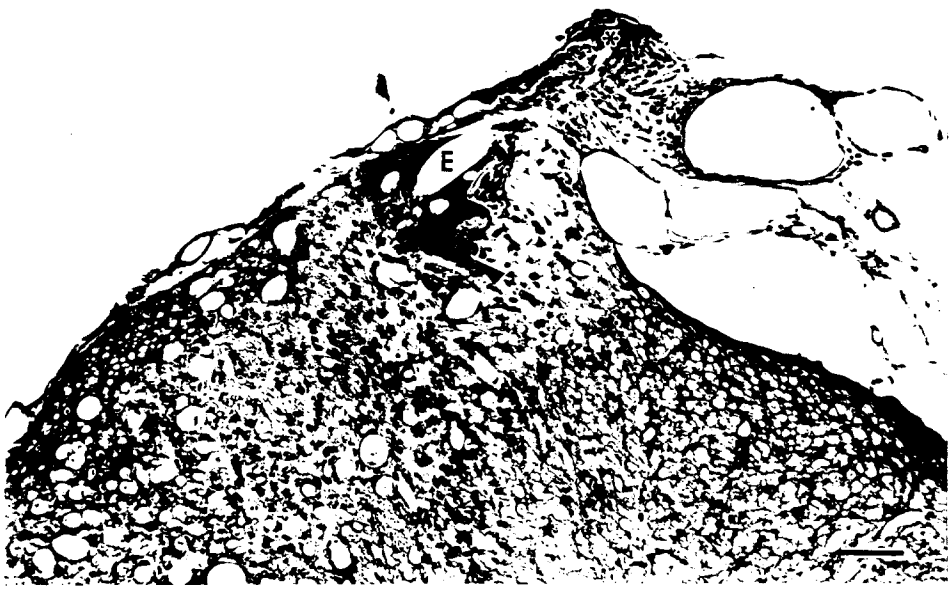

Fig. 9. SP90. The dorsal surface of the spinal cord shows the entrance of an electrode (E) with a large multinucleated giant cell at its edge of the sheath, and what appears to be a large accumulation of astrocytic filaments (arrowhead). Note the apparent meningeal leukocytic infiltrate (*). Bar = 100 μm.

Fig. 10. Sp90. Higher magnification of the electrode sheath (S) from Fig. 9 shows the detailed structure of this multinucleated giant cell. Note the accumulation of filaments in an obliquely cut area through the sheath (*). Bar = 25 μm.

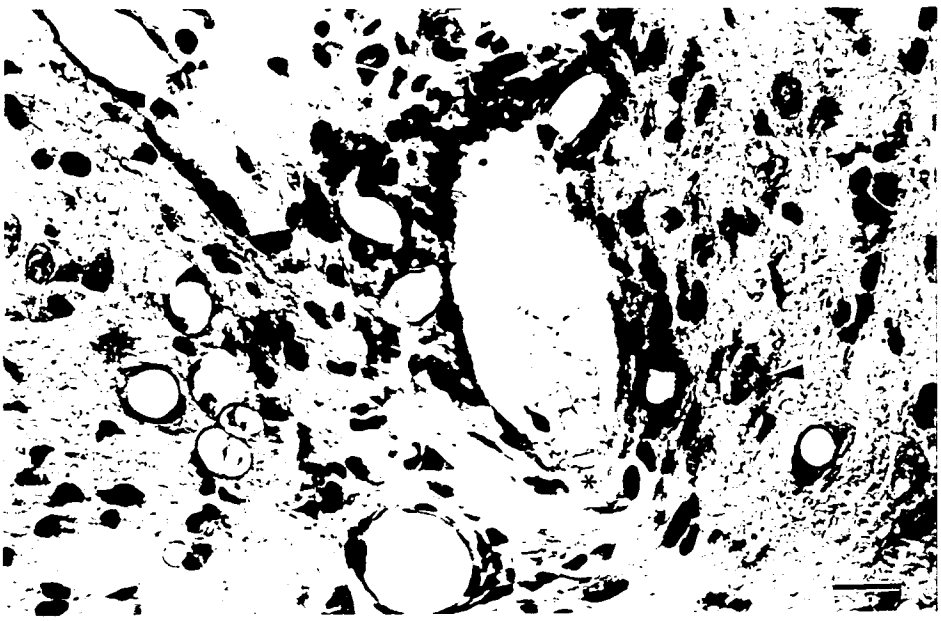

Fig. 11. Sp89. The tip of this electrode (*) demonstrates the appearance of the surrounding tissue. The neurons in this area appear normal (arrowhead) and there is no evidence of leukocyte infiltrate. Bar = 25 μm.

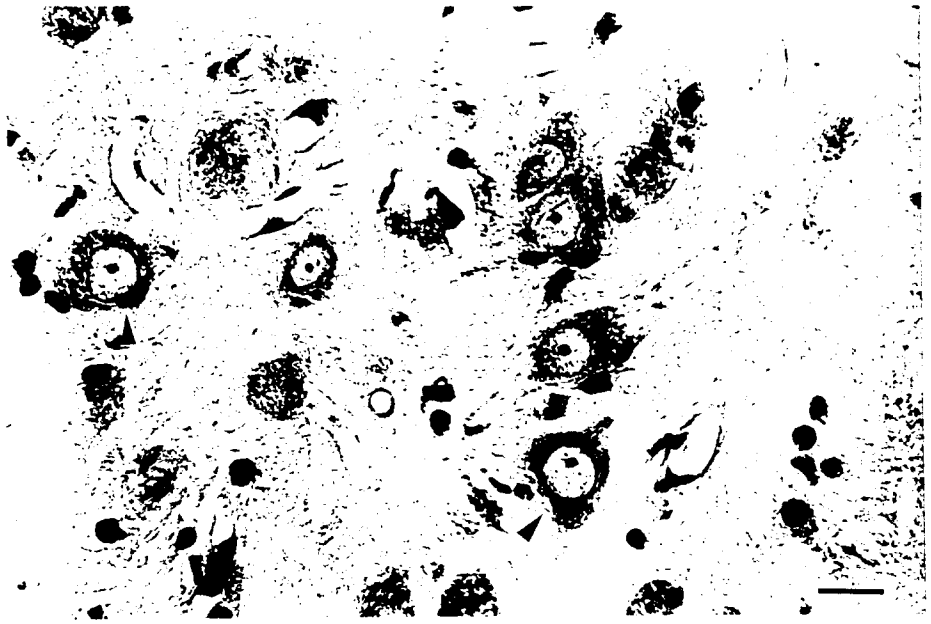

Fig. 12. Sp90. The normal neuronal Nissl stain is shown for the mediolateral gray horn. Note the distribution of the endoplasmic reticulum (arrowheads). Bar = 25 µm.

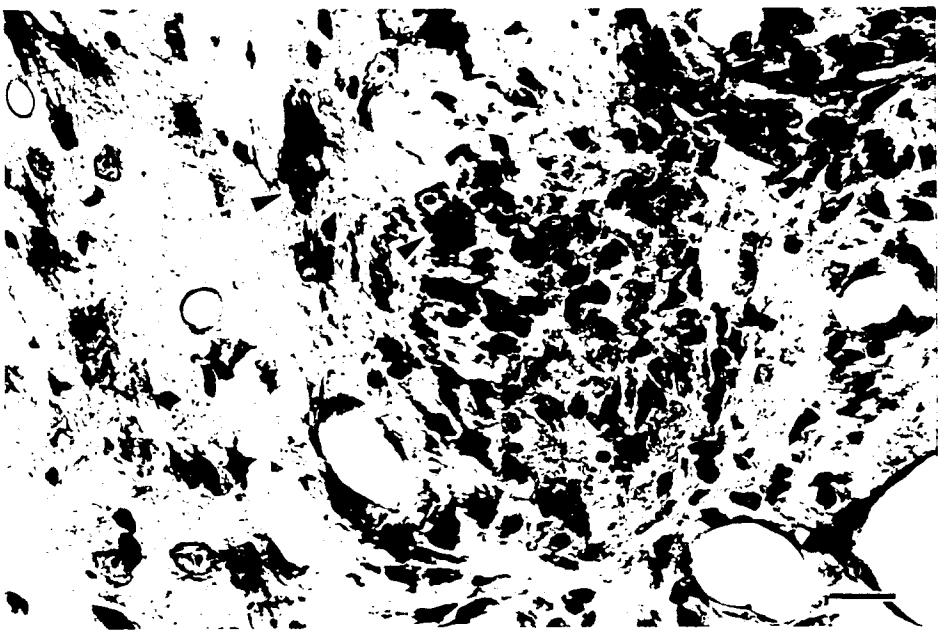

Fig. 13. Sp90. Compared to the normal neurons from the contralateral side of the cord, some small neurons immediately adjacent to the electrodes may show a clumping of the Nissl substance (arrowhead) suggesting possible damage of these cells. These neurons, however, appear reversibly injured. Neurons slightly farther from the electrode tip appear normal. Bar = 25 µm.

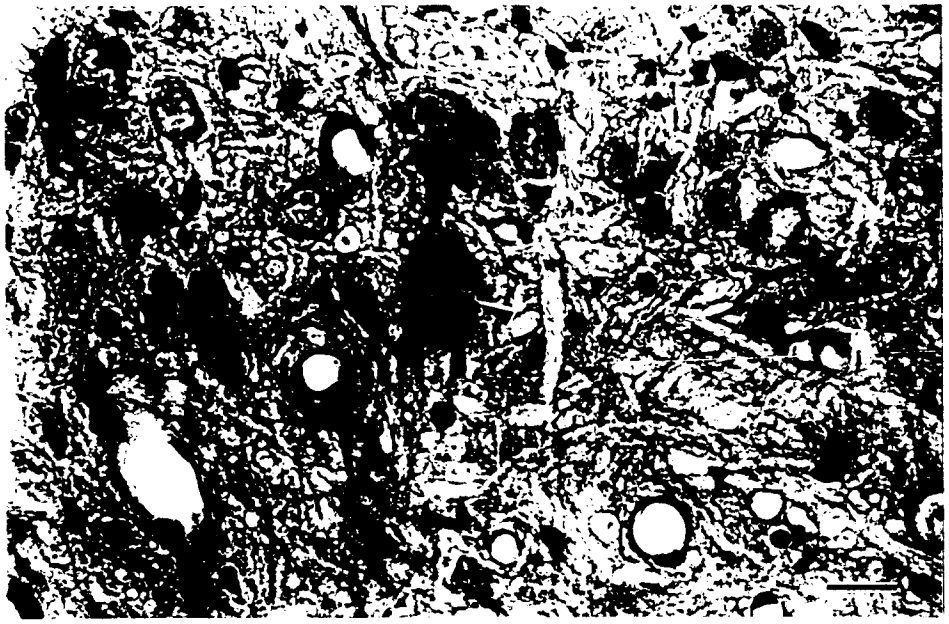

Fig. 14. Sp89. Another Nissl stained gray matter demonstrates an unusual neuron. Note the diffuse appearance of the neuronal soma, and the nucleus and nucleolus are not in the plane of section (arrowhead). Other nearby neurons appear normal (arrowhead). Bar = 25 μm.

Figs.15 -18. Sp89 and sp91. These four micrographs demonstrate the dorsal cord surface near the site where electrodes were inserted. Serial sections illustrate how the pial membrane (*) may be drawn down into the spinal cord at the time of surgical electrode implanting. At the time of sacrifice, there was some infiltration of inflammatory cells. Fig. 15 (sp89) Bar = 200 μm.

Fig. 16. (Sp91). See legend above for Fig. 15. Bar = 100 µm.

Fig. 17. See legend above for Fig. 15. Bar = 100 µm.

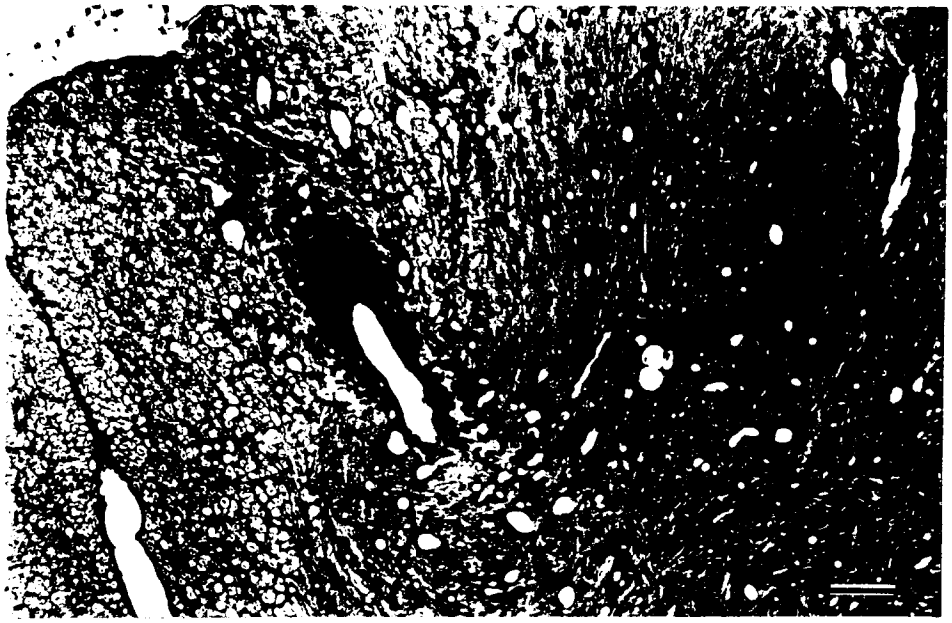

Fig. 18. See legend above for Fig. 15. Bar = 100 µm.